Postprint of: Winiarski M., Mcqueen T., Stabilization of the pyrochlore phase of $Mn_2Sb_2O_7$ by double substitution, JOURNAL OF SOLID STATE CHEMISTRY, Vol. 278 (2019), 120898, DOI: 10.1016/j.jssc.2019.120898

Stabilization of the pyrochlore phase of $Mn_2Sb_2O_7$ by double substitution

M.J. Winiarski[1,2] and T.M. McQueen[1,3,*]

[1] Department of Chemistry, Department of Physics and Astronomy, and Institute for Quantum Matter, Johns Hopkins University, Baltimore, MD, 21231, USA

[2] Faculty of Applied Physics and Mathematics, Gdansk University of Technology, ul. Narutowicza 11/12, 80-233 Gdansk, Poland

[3] Department of Materials Science and Engineering, Johns Hopkins University, Baltimore, MD, 21231, USA

Abstract

Polycrystalline samples of $(Ce^{4+}Mn^{2+}{}_3)(Ga^{3+}Sb^{5+}{}_3)O_{14}$ were synthesized by a high-temperature solid-state reaction. In contrast with the parent $Mn_2Sb_2O_7$ compound that adopts a rhombohedral or monoclinic structure at T > 600 °C, the pyrochlore structure of $CeMn_3GaSb_3O_{14}$ is retained up to at least 1070°C. High-resolution synchrotron x-ray diffraction measurements show no sign of a superstructure or distortion from cubic symmetry in the substituted compound. The stabilization of the pyrochlore structure can be attributed to the effect of configurational disorder due to partial substitution of A and B site. Magnetization and heat capacity data suggest a spin-glass transition below T ≈ 2 K. Our results extends the range of available pyrochlore oxides, and demonstrate that entropic stabilization is a viable route to stabilize novel materials with complex structure types.

Introduction

The pyrochlore compounds are of particular interest in the study of the effects of geometrical frustration on magnetism. A variety of interesting magnetic ground states has been observed in pyrochlores, particularly the spin ice [1,2] and spin liquid [2,3] states. Most of the oxide pyrochlores have either $A^{3+}{}_2B^{4+}{}_2O_7$ or $A^{2+}{}_2B^{5+}{}_2O_7$ site valency [4]. Since only a relatively large cation can occupy the eightfold-coordinate *A* site, most of the magnetic pyrochlore oxide are either based on the moment-bearing trivalent lanthanide ion on the *A* site, or a tetra/pentavalent transition metal (usually 4*d* or 5*d*) on the tetrahedrally-coordinated *B* site [4]. There are however three known oxide pyrochlores with a divalent 3*d* transition metal cation on the *A* site: $Mn_2Sb_2O_7$, $Co_2Sb_2O_7$, and $Ni_2Sb_2O_7$ [5,6].

The high-spin Mn^{2+} ion has a zero orbital angular momentum, making it a purely Heisenberg ion with no orbital constraints on the spin direction [7]. The magnetic ground state of such Heisenberg pyrochlore can be more exotic than the all-in-all-out configuration observed in many of the pyrochlores [7,8].

$Mn_2Sb_2O_7$ oxide was reported to crystallize in a rombohedral or monoclinic structure when prepared via a high-temperature solid-state reaction of MnO and Sb_2O_3 [5,9–11], but can be also obtained in a cubic pyrochlore form via a step-wise low-temperature (T < 600°C) reaction of manganese(II) acetate and hydrated antimony(V) oxide [6,10,11]. It is worth noting that $Mn_2Sb_2O_7$ is one of the two known Mn^{2+} pyrochlores (the other being the $NaSrMn_2F_7$ fluoride with Mn^{2+} on the *B* site [12]). This low-temperature method was also successfully applied to synthesis of the Ni^{2+} and Co^{2+} analogues [6]. $Mn_2Sb_2O_7$ is

particularly unusual because it combines Mn^{2+} and Sb^{5+}, ions that in most cases would be unstable towards electron transfer to generate Mn^{3+} and Sb^{3+}.

Here we report the synthesis of $CeMn_3GaSb_3O_{14}$ oxide, a doubly substituted variant of $Mn_2Sb_2O_7$. In contrast with the parent compound, $CeMn_3GaSb_3O_{14}$ retains the cubic pyrochlore structure when heated up to at least 1070°C, with no observable ordering of the (Ce,Mn) or (Ga,Sb) ion pairs We propose that the stability is enhanced due to an entropic effect, such as observed in high-entropy alloys and related systems. This may have interesting implications on the chemistry and physics of pyrochlores, which are very often found disordered or distorted [13,14].

Experimental procedure

Polycrystalline samples of $CeMn_3GaSb_3O_{14}$ were synthesized by means of a solid state reaction method. Ceric ammonium nitrate ($(NH_4)_2Ce(NO_3)_6$, Alfa Aesar, 99+% pure), manganese(II) oxide (Alfa Aesar, 99.99%), gallium(III) oxide (NOAH Technologies, 99.995%) and antimony(III) oxide (NOAH Technologies, 99.9%) were mixed in stoichiometric amounts and finely-ground using a mortar and pestle and pressed into pellets. Sample 1 was synthesized by first heated to T = 1000˚C at 150˚C/h, held for 15 h, and furnace-cooled to room temperature, then ground, re-pressed, and heated for a total of 64 hours at T = 1070˚C with two intermediate re-grinding steps. Sample 2 was synthesized the same way, but annealed afterwards for 6 days at T = 1000˚C and furnace-cooled to room temperature. Sample 3 was kept for 120h at T = 1070˚C during the synthesis (with intermediate re-grindings), then subjected to annealing for 6 days at T = 1000˚C and 1 day at T = 1070˚C, followed by a slow ramp (20˚C/h) to room temperature. After accounting for the mass loss due to the decomposition of $(NH_4)_2Ce(NO_3)_6$ and gain due to oxidation of Sb^{3+} to Sb^{5+}, the mass changes of samples during annealing were found to be negligible. Laboratory x-ray diffraction patterns of all 3 samples showed that a pure pyrochlore phase was obtained.

Synchrotron XRD (SXRD) patterns were collected at T = 295 K using the 11-BM beamline at Advanced Photon Source, Argonne National Laboratory. Patterns were analyzed by means of Rietveld refinement using the FullProf software package [15]. Simulation of the SXRD pattern for a trigonally-distorted structure was performed using the PowderCell 2.4 program [16]. The amount of impurity phases was quantified using the Rietveld method. The 1:3:1:3 Ce:Mn:Ga:Sb stoichiometry of obtained samples was confirmed using energy dispersive x-ray spectroscopy (EDS) with FEI Quanta 250DFEG scanning electron microscope equipped with an EDAX Apollo-X SDD EDS probe. Collected spectra were processed by means of the standardless eZAF method using the EDAX TEAM software.

Magnetization measurements were carried out on sample 1 using a Quantum Design Physical Properties Measurement System (PPMS) with the ACMS option from T = 2 to 300 K. Magnetic susceptibility was approximated by $\chi = M/H$, where M – measured molar magnetization and H – applied magnetic field. Heat capacity measurements were performed in PPMS by means of the standard semi-adiabatic pulse method.

Results and discussion

High-resolution SXRD data revealed a cubic pyrochlore phase in samples 1 and 2 with < 0.1 wt.% of CeO_2 and $MnSb_2O_4$ [17] impurity phases present. Sample 3 contained slightly higher amount of impurities (~0.8 and ~0.6 wt.%). Rietveld refinements of crystal structures revealed no significant differences between crystal structures of the main phase in samples 1-3 and suggested a statistical distribution of Ce^{4+}/Mn^{2+} and Ga^{3+}/Sb^{5+} ions over the *A* and *B* pyrochlore sites, respectively. Refinement of cation site occupancies yields values close to nominal and does not improve the fit significantly. They were therefore kept fixed in the structural model. Small differences between the unit cell parameters (less than 0.01%) may result from a varying oxygen vacancy concentrations. A Rietveld refinement of the SXRD data is shown in Fig. 1(a,c,d) and the results are presented in Table 1. Unit cell parameter of $CeMn_3GaSb_3O_{14}$ was found to be very close to the $Mn_2Sb_2O_7$ parent compound (a = 10.166 Å [6]).

Table 1 Unit cell parameters and atomic coordinates for $CeMn_3GaSb_3O_{14}$ at T = 295 K as obtained from Rietveld fits to high-resolution SXRD patterns. Conventional background-corrected Rietveld *R* factors for the fit calculated only for points with Bragg contributions [24,25] are: (sample 1) R_p = 7.18%, R_{wp} = 7.77%, R_{exp} = 4.27%, χ^2 = 3.31; (sample 2) R_p = 6.82%, R_{wp} = 7.59%, R_{exp} = 4.27%, χ^2 = 3.16; (sample 3) R_p = 7.68%, R_{wp} = 8.85%, R_{exp} = 4.42%, χ^2 = 4.01.

Formula:	$(Ce_{0.25}Mn_{0.75})_2(Ga_{0.25}Sb_{0.75})_2O_7$			
Space group:	F d -3 m (no. 227), setting 2			
a (Å)	*1*: 10.1382(1), *2*: 10.1377(1), *3*: 10.1396(1)			
Unit cell volume (Å^3)	1042			
No. formula units / unit cell	8			
Formula weight (g/mol)	481.96			
Calculated density (g/cm^3)	6.14			
	x	y	z	B (Å^2)
Ce (s.o.f. = 0.25) Mn (s.o.f. = 0.75)	½	½	½	*Sample 1*: 0.774(3) *Sample 2*: 0.771(3) *Sample 3*: 0.807(3)
Ga (s.o.f. = 0.25) Sb (s.o.f. = 0.75)	0	0	0	*Sample 1*: 0.303(1) *Sample 2*: 0.315(2) *Sample 3*: 0.279(1)
O1	*Sample 1*: 0.3272(1) *Sample 2*: 0.3273(1) *Sample 3*: 0.3265(1)	1/8	1/8	*Sample 1*: 0.45(2) *Sample 2*: 0.45(2) *Sample 3*: 0.41(2)
O2	3/8	3/8	3/8	*Sample 1*: 0.31(3) *Sample 2*: 0.30(3) *Sample 3*: 0.33(3)

Bond lengths and results of bond valence analysis are gathered in Table 2. The calculated bond valence sums (BVS) are in agreement with assumed valence states (Ce^{4+}, Mn^{2+}, Ga^{3+}, Sb^{5+}), although the *A* site ions (Ce and Mn) are underbonded by approx. 25% and O2 by approx.. 20%. Such effect is also observed in the cubic variant of $Mn_2Sb_2O_7$ and is discussed below. If Ce is assumed in the +3 state, the percentage discrepancy between the assumed valency and BVS is significantly higher (~35%), supporting the Ce^{4+} scenario.

Peak shapes were well-described using the Thompson-Cox-Hastings pseudo-Voigt function [18,19], with no anisotropic broadening observed. Isotropic crystallite size broadening of peaks was found to be

negligible, corresponding to an apparent crystallite size of > 2000 nm, and the obtained strain was found to be 2.0% in case of Samples 1 and 2 and 2.2% in sample 3.

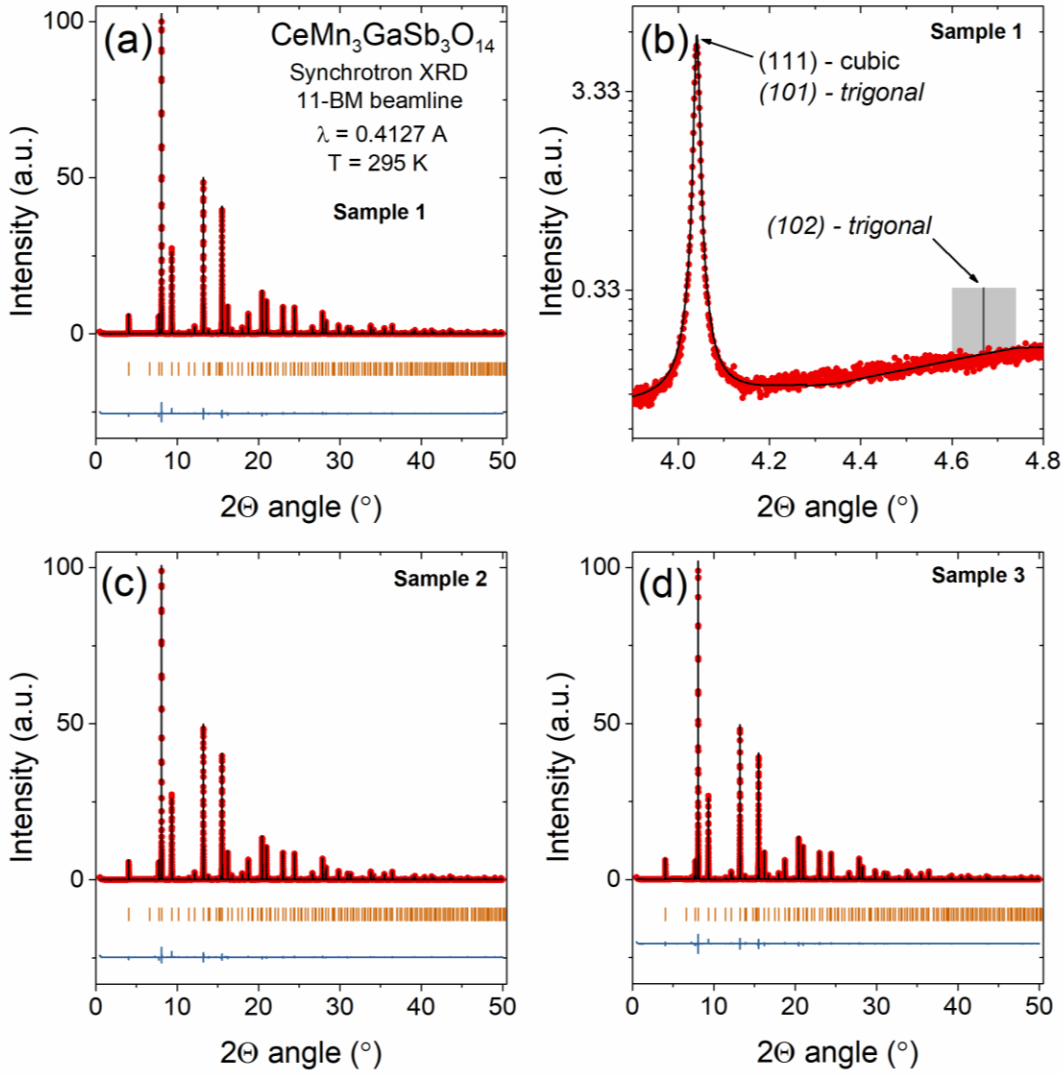

Figure 1 (a,c,d) Rietveld fit (black line) to the SXRD pattern of $CeMn_3GaSb_3O_{14}$ collected at T = 295 K (red points). Blue line shows the difference between observed and calculated intensities. Orange ticks mark the expected positions of Bragg reflections for the cubic pyrochlore phase. Enlarged patterns are presented in the Supplementary Material. Panel (b) shows the expected position of the (102) reflection of a simulated, ordered R-3*m* phase (grey rectangle). Height of the rectangle corresponds to the simulated peak intensity for a model assuming complete ordering. Note that the (102) peak is also expected for the rhombohedral variant of $Mn_2Sb_2O_7$.

An ordered substitution of ¼ sites of a pyrochlore lattice results in a kagomé lattice, as it was recently shown in $Ln_3Sb_3M_2O_{14}$ (*Ln* – lanthanides, *M* = Mg, Ca, Co, Zn) oxides [20–23]. This is realized by breaking the cubic pyrochlore symmetry (space group F*d*-3*m*, no. 227) via a *translationengleiche* transformation to trigonal R-3*m*, no. 166 in which the pyrochlore 16*c* and 16*d* Wyckoff sites are split into 3*a* + 9*d* and 3*b* + 9*c* pairs. In our case, however, no superstructure reflections (see Fig. 1(b)), peak splittings, or anisotropic peak asymmetry consistent with rhombohedral or monoclinic distortions were observed within the resolution of the SXRD. The *A* and *B* site disorder is likely caused by a close similarity of ionic radii of Ce^{4+}/Mn^{2+} and Ga^{3+}/Sb^{5+} (see Table 3).

Table 2 Summary of bond lengths and bond valence analysis for the refined structure models. Bond valency for Ce is calculated assuming the +4 valence state. Assuming a +3 valency for Ce yields BVS of 4.06 for all three samples.

Bond lengths:	**Sample 1**	**Sample 2**	**Sample 3**
Ce/Mn – O1 (x 6)	2.506(1)	2.505(1)	2.512(1)
Ce/Mn – O2 (x 2)	2.195(1)	2.195(1)	2.195(1)
Average	2.428	2.428	2.433
Ga/Sb – O1 (x 6)	1.956(1)	1.956(1)	1.953(1)
Bond valence:	**Sample 1**	**Sample 2**	**Sample 3**
Ce – O1 (x 6)	0.28	0.28	0.27
Ce – O2 (x 2)	0.64	0.64	0.64
BVS for Ce^{4+}:	2.96	2.96	2.90
Mn – O1 (x 6)	0.14	0.15	0.14
Mn – O2 (x 2)	0.33	0.33	0.33
BVS for Mn^{2+}	1.50	1.56	1.50
Ga – O1 (x 6)	0.54	0.54	0.55
BVS for Ga^{3+}	3.24	3.26	3.30
Sb – O1 (x 6)	0.96	0.96	0.97
BVS for Sb^{5+}	5.76	5.76	5.82
O1 – Ce (x 2)	0.07	0.07	0.07
O1 – Mn (x 2)	0.11	0.11	0.11
O1 – Ga (x 2)	0.14	0.14	0.14
O1 – Sb (x 2)	0.72	0.72	0.73
BVS for $O1^{2-}$	2.08	2.08	2.10
O2 – Ce (x 4)	0.16	0.16	0.16
O2 – Mn (x 4)	0.25	0.25	0.25
BVS for $O2^{2-}$	1.64	1.64	1.64

Table 3 Ionic radii of Ce, Mn, Ga, and Sb for CN =6 and 8. Values were taken from ref. [26]. The most likely oxidation states of elements in the $CeMn_3GaSb_3O_{14}$ compound are highlighted in bold. HS and LS stands for high- and low-spin configurations, respectively.

	r_{ion} (Å), CN = 6	r_{ion} (Å), CN = 8
Ce^{3+}	1.01	1.14
Ce^{4+}	0.87	**0.97**
Mn^{2+}	0.67 (LS) / 0.81 (HS)	**0.96**
Mn^{3+}	0.58 (LS) / 0.65 (HS)	-
Ga^{3+}	**0.62**	-
Sb^{3+}	0.76	-
Sb^{5+}	**0.60**	-

As it was discussed by Subramanian *et al*. [5] the rhombohedral distortion in $Mn_2Sb_2O_7$ is caused by a small size of Mn^{2+} ion compared to oxygen atoms in its coordination sphere. This is highlighted by the bond valence sum (BVS) which for Mn^{2+} in pyrochlore $Mn_2Sb_2O_7$ has a value of 1.64 which is about 18% lower than expected. In fact, Mn^{2+} is one of the smallest cations for which a $A^{2+}{}_2B^{5+}{}_2O_7$ pyrochlore phase was reported [4] (the only smaller ions being Co^{2+} and Ni^{2+} [6]). One may thus argue that the stabilization of the pyrochlore structure in $CeMn_3GaSb_3O_{14}$ arises from a "chemical pressure" effects, but the ratio of effective ionic radii in case of the substituted compound is even lower than for the parent (1.59 vs. 1.60), due to the introduction of the slightly larger Ga^{3+} in the place of Sb^{5+} (see Table 3). In $CeMn_3GaSb_3O_{14}$ the

underbonding of cations at the *A* site is even more pronounced, with BVS for Mn^{2+} around 1.5 (~25% lower than expected; see Table 2), which would suggest that the pyrochlore structure should be even less stable in the substituted compound.

Cai and Nino [27] proposed a stability criterion for pyrochlore/weberite structure based on the ratios of ionic radii of A- and B-site cations ($x_r = r_A/r_B$) and electronegativities ($x_I = I_A/(I_A+I_B)$, where $I_{el} = 1- \exp(-0.25(\chi_{el}-\chi_O))$, χ_{el} and χ_O being electronegativity of the element and of oxygen, respectively). With $x_r = 1.60$ and $x_I = 0.54$, $Mn_2Sb_2O_7$ lies close to the proposed stability line for pyrochlore structure, which is in line with the metastability of pyrochlore phase (electronegativity values were taken from refs. [28,29]). In case of $CeMn_3GaSb_3O_{14}$ the $x_r = 1.59$ and $x_I = 0.56$ values also position the compound in the vicinity of the phase stability line, although already on the weberite side. For comparison, the $Ni_2Sb_2O_7$ and $Co_2Sb_2O_7$ compounds [6] lie well within the pyrochlore region and in fact they were not reported to form in any variant of the weberite structure.

These considerations suggest that neither the ionic size nor electronegativity difference plays a major role in stabilization of the pyrochlore phase by substitution. The increased stability of pyrochlore may however arise from entropic stabilization effect [30]. Such phenomenon was observed in the family of high-entropy alloys [31,32] and recently also in binary oxides [30]. The possibility of entropic stabilization in a complex pyrochlore system is interesting and should be studied in more detail.

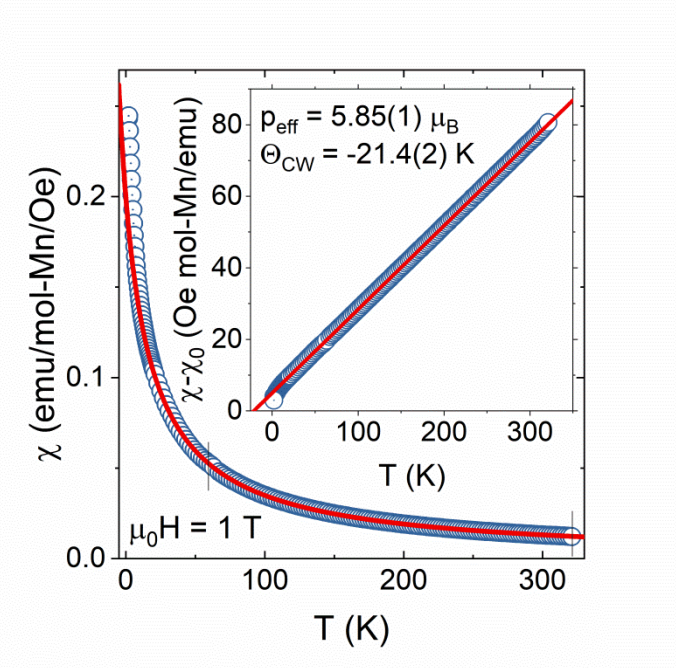

Figure 2 DC magnetic susceptibility of $CeMn_3GaSb_3O_{14}$ (sample 1). Red line is a Curie-Weiss fit to the susceptibility at μ_0H = 1 T applied magnetic field (black horizontal ticks mark the fitting region). Inset shows the inverse susceptibility corrected for the diamagnetic temperature-independent contribution, showing linear C-W relation down to approx. 20 K.

DC magnetization measurements (Fig. 2) show Curie-Weiss (C-W) paramagnetic behavior between 20 and 320 K, with a slight deviation starting below 20 K. Fit to the magnetic susceptibility (60-320 K) yielded the C-W temperature Θ_{C-W} = -21.4(2) K and effective magnetic moment of 5.85(1) μ_B/Mn atom, consistent with the spin-only value for high-spin Mn^{2+} (5.92 μ_B [33]). This further supports the assumed valency of Mn and

Ce (as Ce^{4+} is diamagnetic). The interactions are weaker compared to both the cubic pyrochlore and rhombohedral variants of $Mn_2Sb_2O_7$ where they are of the order of 40-50 K [6,7,34,35]. This is likely due to the introduced disorder, particularly at the *A* site, as well as due to dilution of moment-bearing Mn^{2+} ions with diamagnetic Ce^{4+}.

Low-field DC magnetization measurements (Fig. 3) shows no sign of spin-glass transition in $CeMn_3GaSb_3O_{14}$ down to 2 K, however a small upturn is seen in AC susceptibility around 2.2 K (see the inset of Fig. 3), which is likely due to the presence of spin-glass transition at a temperature just below 2 K. The spin-freezing temperature is then suppressed by a factor of approx. 2.5 compared to the pyrochlore $Mn_2Sb_2O_7$ (T_{sg} = 5.5 K), in agreement with interactions in the substituted compound weaker by a similar factor. It is worth noting that previously reported $T_{sg} \approx 40$ K for $Mn_2Sb_2O_7$ is likely due to the presence of an Mn_3O_4 impurity phase [7].

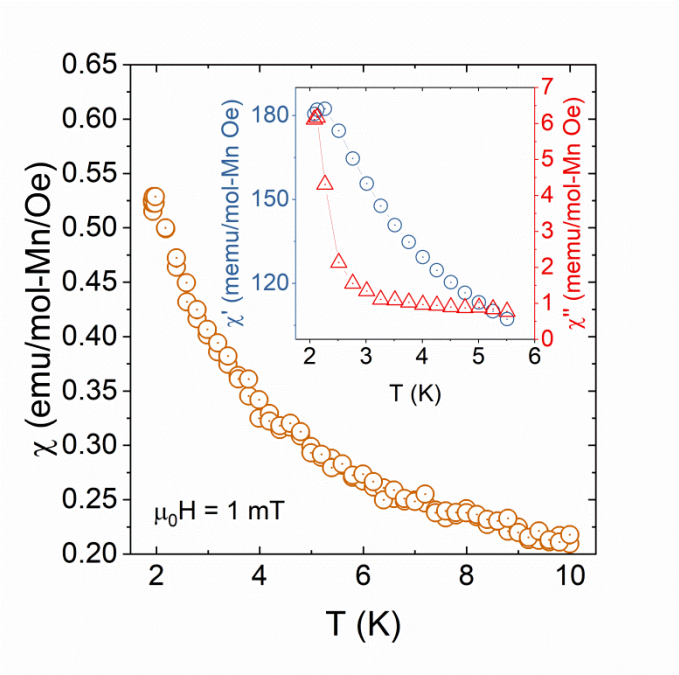

Figure 3 Low-field (μ_0H = 1 mT) magnetic susceptibility in the low-temperature region, showing no sign of magnetic ordering down to T = 2 K. Inset shows real and imaginary part of AC susceptibility measured at μ_0H_{dc} = 0.5 mT applied field with μ_0H_{ac} = 0.3 mT, f = 1 kHz excitations. A small upturn of susceptibility is seen around T = 2 K, likely resulting from the vicinity of a spin-glass transition.

Heat capacity measurements (Fig 4) reveal an anomaly centered at $T \approx 6$ K. The phonon contribution to heat capacity of $CeMn_3GaSb_3O_{14}$ is expected to be similar as in the weberite $Sr_2Sb_2O_7$ (the distortion from a cubic pyrochlore lattice in the latter compound is small enough to enable this approximation). The magnetic contribution (C_{mag}) was thus obtained by subtraction of the experimental heat capacity of $Sr_2Sb_2O_7$ [35] and is presented in Fig. 4(a). Integration of C_{mag}/T yields the magnetic entropy, which saturates above $T \approx 50$ K at a value slightly lower than expected for a Mn^{2+} S = 5/2 system (R ln 6). This can be partially attributed to the error introduced by the subtraction of the lattice heat capacity approximant and the lack of data below T = 2 K, but can also be attributed to a remnant magnetic disorder (as in the case of $Mn_3Al_2Si_3O_{12}$ [36]).

While the AC magnetization suggest the spin-glass transition just below T = 2 K, the heat capacity peak is centered around T = 6 K. Such difference is a typical feature of spin glass systems [37].

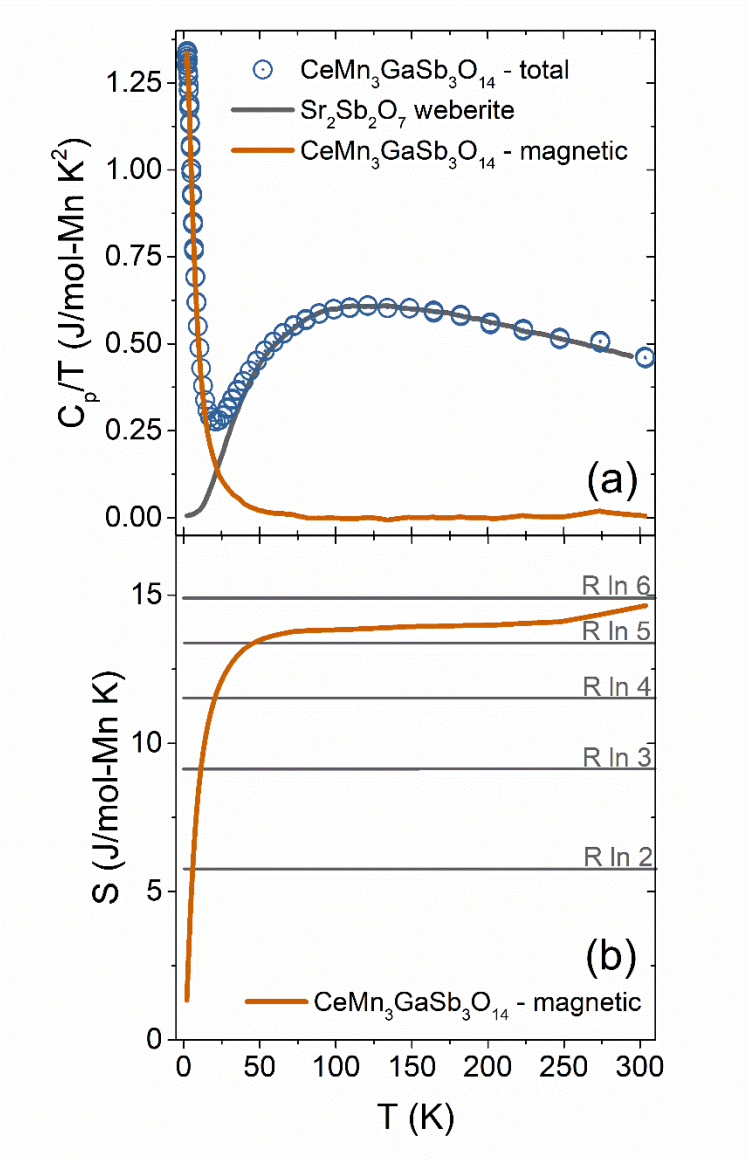

Figure 4 (a) Total heat capacity of $CeMn_3GaSb_3O_{14}$ (blue circles). The phonon part was approximated using the experimental heat capacity of $Sr_2Sb_2O_7$ weberite [35] (gray line). Orange line shows the extracted magnetic heat capacity contribution. Panel (b) shows the estimated magnetic entropy, saturating above T = 50 K at a value between R ln 5 and R ln 6.

Conclusions

We have synthesized a double-substituted oxide $CeMn_3GaSb_3O_{14}$. Magnetization and heat capacity data supports the assumed valencies of elements: Ce^{4+}, Mn^{2+}, Ga^{3+}, and Sb^{5+}. $CeMn_3GaSb_3O_{14}$ is likely a spin-glass system, similarly to the $Mn_2Sb_2O_7$ pyrochlore, but with weaker magnetic interactions (by a factor of ~2) and suppressed transition temperature.

High-resolution SXRD data show that the compound retains the cubic pyrochlore structure even after prolonged heating at T = 1070°C. This is in contrast with the parent $Mn_2Sb_2O_7$ phase, which distorts to a rhombohedral weberite-type structure when heated above T = 600°C [6,10,11]. We attribute this effect to the configurational disorder resulting from partial substitution, as the analysis of relative ionic radii and electronegativities could not explain the stabilization. Such entropic stabilization mechanism was proposed as an explanation of the stability of high-entropy alloys [31] and mixed oxides [30]. This disorder-driven stabilization may be a way to preserve a structurally perfect pyrochlore lattice in systems that are prone to distortion [14].

Acknowledgements

This work was supported as part of the Institute for the Quantum Matter, an Energy Frontier Research Center funded by the US Department of Energy, Office of Science, Office of Basic Energy Sciences, under award DE-SC0019331.

Use of the Advanced Photon Source at Argonne National Laboratory was supported by the US Department of Energy, Office of Science, Office of Basic Energy Sciences, under Contract No. DE-AC02-06CH11357.

M.J. Winiarski was supported by the Foundation for Polish Science (FNP).

References

[1] S.T. Bramwell, M.J.P. Gingras, Spin Ice State in Frustrated Magnetic Pyrochlore Materials, Science. 294 (2001) 1495–1501.
[2] M.J.P. Gingras, P.A. McClarty, Quantum spin ice: a search for gapless quantum spin liquids in pyrochlore magnets, Rep. Prog. Phys. 77 (2014) 056501.
[3] R. Sibille, E. Lhotel, V. Pomjakushin, C. Baines, T. Fennell, M. Kenzelmann, Candidate Quantum Spin Liquid in the Ce3+ Pyrochlore Stannate Ce2Sn2O7, Phys. Rev. Lett. 115 (2015) 097202.
[4] M.A. Subramanian, G. Aravamudan, G.V. Subba Rao, Oxide pyrochlores — A review, Prog. Solid State Ch. 15 (1983) 55–143.
[7] M.A. Subramanian, A. Clearfield, A.M. Umarji, G.K. Shenoy, G.V.S. Rao, Synthesis and solid state studies on Mb2Sb2O7 and (Mn1-xCdx)2Sb2O7 pyrochlores, J. Solid State Chem. 52 (1984) 124–129.
[11] H.D. Zhou, C.R. Wiebe, J.A. Janik, B. Vogt, A. Harter, N.S. Dalal, J.S. Gardner, Spin glass transitions in the absence of chemical disorder for the pyrochlores A2Sb2O7 (A=Mn, Co, Ni), J. Solid State Chem. 183 (2010) 890–894.
[5] D.C. Peets, H. Sim, M. Avdeev, J.-G. Park, 3d-electron Heisenberg pyrochlore Mn2Sb2O7, Phys. Rev. B. 94 (2016) 174431.
[6] Y. Wan, M.J.P. Gingras, Color ice states, weathervane modes, and order by disorder in the bilinear-biquadratic pyrochlore Heisenberg antiferromagnet, Phys. Rev. B. 94 (2016) 174417.
[8] H.G. Scott, Synthesis and crystal structures of the manganous antimonates Mn2Sb2O7 and MnSb2O6, J. Solid State Chem. 66 (1987) 171–180.
[9] L. Chelazzi, T. Boffa Ballaran, G.O. Lepore, L. Bindi, P. Bonazzi, High-pressure behaviour of synthetic weberite-type Mn2+2Sb5+2O7: An in situ single-crystal X-ray study, Solid State Sci. 21 (2013) 85–90.

[10] D.C. Peets, H. Sim, M. Avdeev, Optimizing the Preparation of Monoclinic and Pyrochlore Mn2Sb2O7, J. Phys.: Conf. Ser. 807 (2017) 042002.
[12] M.B. Sanders, J.W. Krizan, K.W. Plumb, T.M. McQueen, R.J. Cava, NaSrMn2F7 , NaCaFe2F7 , and NaSrFe2F7 : novel single crystal pyrochlore antiferromagnets, J. Phys.: Condens. Matter. 29 (2017) 045801.
[13] K.E. Arpino, B.A. Trump, A.O. Scheie, T.M. McQueen, S.M. Koohpayeh, Impact of stoichiometry of Yb2Ti2O7 on its physical properties, Phys. Rev. B. 95 (2017) 094407.
[14] B.A. Trump, S.M. Koohpayeh, K.J.T. Livi, J.-J. Wen, K.E. Arpino, Q.M. Ramasse, R. Brydson, M. Feygenson, H. Takeda, M. Takigawa, K. Kimura, S. Nakatsuji, C.L. Broholm, T.M. McQueen, Universal geometric frustration in pyrochlores, Nat. Commun.. 9 (2018) 2619.
[15] J. Rodríguez-Carvajal, Recent advances in magnetic structure determination by neutron powder diffraction, Physica B. 192 (1993) 55–69.
[16] W. Kraus, G. Nolze, POWDER CELL – a program for the representation and manipulation of crystal structures and calculation of the resulting X-ray powder patterns, J. Appl. Cryst. 29 (1996) 301–303.
[16] R. Chater, J.R. Gavarri, Evolution structure entre 2 et 300 K de l'oxyde MnSb2O4: Proprie´te´se´lastiques et magne´tiques anisotropes, J. Solid State Chem. 59 (1985) 123–131.
[17] P. Thompson, D.E. Cox, J.B. Hastings, Rietveld refinement of Debye–Scherrer synchrotron X-ray data from Al2O3, J. Appl. Cryst. 20 (1987) 79–83.
[18] J. Rodríquez-Carvajal, T. Roisnel, Line broadening analysis using FullProf: determination of microstructural properties, Mater. Sci. Forum. 443 (2004) 123–126.
[21] K. Li, Y. Hu, Y. Wang, T. Kamiyama, B. Wang, Z. Li, J. Lin, Syntheses and properties of a family of new compounds RE3Sb3Co2O14 (RE=La, Pr, Nd, Sm–Ho) with an ordered pyrochlore structure, J. Solid State Chem. 217 (2014) 80–86.
[22] W.T. Fu, D.J.W. IJdo, New rhombohedral pyrochlores Ca2Ln3Sb3O14 (Ln=lanthanide and Y): Space group revised, J. Solid State Chem. 229 (2015) 330–335.
[23] M. B. Sanders, J. W. Krizan, R. J. Cava, RE3Sb3Zn2O14 (RE = La, Pr, Nd, Sm, Eu, Gd): a new family of pyrochlore derivatives with rare earth ions on a 2D Kagome lattice, J. Mater. Chem. C. 4 (2016) 541–550.
[23] M.B. Sanders, K.M. Baroudi, J.W. Krizan, O.A. Mukadam, R.J. Cava, Synthesis, crystal structure, and magnetic properties of novel 2D kagome materials RE3Sb3Mg2O14 (RE = La, Pr, Sm, Eu, Tb, Ho): Comparison to RE3Sb3Zn2O14 family, Phys. Status Solidi B. 253 (2016) 2056–2065.
[19] B.H. Toby, R factors in Rietveld analysis: How good is good enough?, Powder Diffr. 21 (2006) 67–70.
[25] J. Huot, R. Černý, Neutron Powder Diffraction, in: H. Fritzsche, J. Huot, D. Fruchart (Eds.), Neutron Scattering and Other Nuclear Techniques for Hydrogen in Materials, Springer International Publishing, 2016: pp. 31–89.
[26] R.D. Shannon, Revised effective ionic radii and systematic studies of interatomic distances in halides and chalcogenides, Acta Cryst A. 32 (1976) 751–767.
[27] L. Cai, J.C. Nino, Complex ceramic structures. I. Weberites, Acta Cryst. B. 65 (2009) 269–290.
[27] A.L. Allred, E.G. Rochow, A scale of electronegativity based on electrostatic force, J. Inorg. Nucl. Chem. 5 (1958) 264–268.
[29] E.J. Little, M.M. Jones, A complete table of electronegativities, J. Chem. Educ. 37 (1960) 231.
[29] C.M. Rost, E. Sachet, T. Borman, A. Moballegh, E.C. Dickey, D. Hou, J.L. Jones, S. Curtarolo, J.-P. Maria, Entropy-stabilized oxides, Nat. Commun.. 6 (2015) 8485.
[30] Y.F. Ye, Q. Wang, J. Lu, C.T. Liu, Y. Yang, High-entropy alloy: challenges and prospects, Mater. Today. 19 (2016) 349–362.
[32] F. von Rohr, M.J. Winiarski, J. Tao, T. Klimczuk, R.J. Cava, Effect of electron count and chemical complexity in the Ta-Nb-Hf-Zr-Ti high-entropy alloy superconductor, PNAS. 113 (2016) E7144–E7150.
[32] Charles Kittel, Introduction to Solid State Physics, 8th Edition, Wiley, Hoboken, 2004.

[33] H.D. Zhou, C.R. Wiebe, A. Harter, N.S. Dalal, J.S. Gardner, Unconventional spin glass behavior in the cubic pyrochlore $Mn_2Sb_2O_7$, J. Phys.-Condens. Mat. 20 (2008) 325201.
[34] D.C. Peets, H. Sim, S. Choi, M. Avdeev, S. Lee, S.J. Kim, H. Kang, D. Ahn, J.-G. Park, Magnetic transitions in the chiral armchair-kagome system Mn2Sb2O7, Phys. Rev. B. 95 (2017) 014424.
[35] G.C. Lau, T. Klimczuk, F. Ronning, T.M. McQueen, R.J. Cava, Magnetic properties of the garnet and glass forms of Mn3Al2Si3O12, Phys. Rev. B. 80 (2009) 214414.
[37] J.A. Mydosh, Spin glasses: redux: an updated experimental/materials survey, Rep. Prog. Phys. 78 (2015) 052501.